RSC Advances

PAPER

View Article Online
View Journal | View Issue

Cite this: *RSC Adv.*, 2019, **9**, 26880

Evaluation of the performance and emission and spectroscopic analysis of an improved soy methyl ester

S. M. Mozammil Hasnain and R. P. Sharma *

Herein, the performance, emission and physiochemical properties of a soy methyl ester (SME) and its combination with methyl oleate (MO) in a common rail direct injection (CRDI) engine were investigated. Moreover, the performance of the engine in terms of brake power (BP), brake thermal efficiency (BTE), brake specific fuel consumption (BSFC) and NO_x emission was assessed to compute the characteristics of the combination of SME with MO; the reasons for using MO in the blending process were the better ignition quality, oxidative stability and low-temperature flow properties of MO, striking a balance between oxidative stability and low flow properties. A remarkable reduction in the BSFC and an increase in the BTE were found in the blended biodiesel (S80-MO20, S70-M30, and S50-M50) as compared to the case of SME. The blended biodiesel was also characterized by Fourier transform infrared spectroscopy (FTIR), ultraviolet-visible spectroscopy (UV-vis) and nuclear magnetic resonance (NMR) spectroscopy. In the FTIR spectra, a peak was observed at 1745 cm^{-1}, confirming the presence of a triglyceride ester linkage. Since UV-vis spectroscopy is an affordable technique, herein, it has been employed to detect the presence of conjugated dienes in the oxidized biodiesel. The linear line fitted for absorbance *versus* the percentage of the blended fuel at 320 nm showed a high coefficient of determination (R^2 = 0.9454). In addition, H NMR spectroscopy was employed to study the oxidative stability of the blended fuel. Different functional groups with their respective peaks (in ppm) are indicated in the NMR spectra.

Received 10th June 2019
Accepted 8th August 2019

DOI: 10.1039/c9ra04342j

rsc.li/rsc-advances

1. Introduction

Biodiesel is an alternative fuel because of its renewability, carbon neutrality, nontoxicity and biodegradability. Biodiesel contains reactive unsaturated fatty acid esters, mainly oleate and linoleate, which are susceptible to oxidative degradation during the storage process.[1] This degradation results in poor engine performance such as the dilution of engine and seal swelling of the elastomer.[2] The major change occurs in the peroxide value that measures hydro peroxides, which decompose to ketones, acids, oligomers, *etc.*[3]

Bacha *et al.* have investigated that the monitoring of biodiesel oxidative degradation should be mainly conducted by Fourier transform infrared spectroscopy (FTIR); the absorption peak around 1745 cm^{-1} is due to presence of an ester carbonyl group.[4] Faragun *et al.* have observed that the correlation between concentration and FTIR absorption is highly linear (R^2 above 0.993, in most cases 0.999).[5] Shimamoto & Tubino have studied the presence of conjugated dienes in an oxidized biodiesel using UV-vis spectroscopy and found a positive correlation between the peroxide value and UV absorbance.[6] Ghesti *et al.* have indicated that nuclear magnetic resonance (NMR) spectroscopy is the most powerful technique to determine the chemical structure of compounds involved in biodiesel synthesis.[7] In addition, the NMR technique has been used for the quantification of biodiesel in diesel–biodiesel blends.[6] Knothe has reported the peaks of methyl ester (3.6–3.7 ppm), olefin protons (5.3–5.4 ppm), and methyl protons of the hydrocarbon moieties in biodiesel to investigate biodiesel–diesel blends;[8] Monteiro *et al.* have analyzed the usefulness of ^{1}H NMR spectroscopy in the investigation of a blend of methyl biodiesel with diesel fuels using soybean and castor oil biodiesel samples and three diesel fuel samples.[9]

Anderson and Franz have demonstrated the use of NMR spectroscopy for the investigation of the formation of triacylglycerols and FAME during biodiesel production.[10] Satyarthi *et al.* have applied NMR spectroscopy to determine the free fatty acid value (FFA). The authors have used R–CH_2 of FFA and ester to estimate the FFA content.[11] In previous studies, it has been reported that biodiesel emits less CO and particulate matter and causes an insignificant increase in the NO concentration in the atmosphere when compared with diesel;[12,13] reduction in the NO_x emissions can also be achieved by the modification of engine parameters and introduction of metal-based additives.[14]

Department of Mechanical Engineering, Birla Institute of Technology, Ranchi, Jharkhand, India. E-mail: smmh.429@gmail.com; sharmabit47@gmail.com

Kannan has analyzed metal-based additives as oxidation catalysts and found that these additives decrease the oxidation temperature, resulting in the reduction of NO_x emission.[15] Ganesan & Mahalingam have indicated that the addition of nano additives reduces fuel consumption, improves thermal efficiency and releases energy during combustion.[16] Altaie has analyzed the emission performance of a palm oil methyl ester (PME) blended with methyl oleate (MO) (50 : 50 ratio) and found enhanced engine performance due to low calorific value and high kinematic viscosity of the blended biodiesel. The author has also reported that in a diesel engine, only 20% of PME50 : MO50 is mixed with petro-diesel without any modifications.[17]

Many studies have been conducted to understand the physiochemical properties of methyl esters. These studies have reported better ignition qualities, fuel stability and low flow properties, mainly attributed to the presence of monounsaturated fatty acid components such as MO. MO has better ignition quality, oxidative stability and low-temperature flow properties. Similar to other monounsaturated fatty acids, MO strikes a balance between the oxidative stability and low flow properties. Polyunsaturated fatty acids have better cold flow properties but poor fuel stability.[18–20] Knothe has estimated that the cetane number (CN) of MO is between 56 and 59.[21] Lai *et al.* have shown that the SME ignition quality is superior because of the presence of saturated bonds and short-length carbon chains.[22]

In the present study, a soy methyl ester (SME) was blended with MO to investigate the engine performance and emission characteristics. The SME and its blends were also characterized using different techniques such as FTIR, UV and NMR spectroscopies. The novelty of this study is that the blend of SME with MO at higher percentages has been used in the emission performance test in an advanced developed automatic common rail direct injection (CRDI) engine without any engine modification. The characterization of all the blended fuel samples provided the chemical composition of the fuel, which retained the characteristics of diesel.

2. Materials and methods

SME was procured from M/s Ensure Biodiesel from Uttar Pradesh, India. Diesel was purchased from Indian Oil, Ranchi, which is used commercially. The reason behind purchasing the commercially used biodiesel was its ample availability and usage. MO (>65%-technical grade) was purchased from Thermo Fisher. Technical grade MO contains oleate methyl esters as the major constituent along with laurate, myristate, stearate, palmitate, palmitoleate and linoleate as the minor constituents. The NMR solvent $CDCl_3$ was obtained from Sigma Aldrich (99%). The hexane fraction from petroleum (99%) was obtained from Emplura.

SME was blended with MO in the ratios of 80 : 20, 70 : 30 and 50 : 50 for the evaluation of the performance, emissions and physio-chemical characteristics. The characterization of SME and its blended fuel was also performed by FTIR spectroscopy (Make – Shimadzu Corp, spectrometer in the wavenumber range of 7500–350 cm^{-1}), UV-vis spectroscopy (Make – PerkinElmer Lambda 25 UV/vis spectrometer in the wavelength range of 1100–190 nm with a 10 mm quartz cuvette at room temperature) and NMR spectroscopy (Make – JEOL JNM spectrometer, at 298 K). The absorption spectra of all samples were obtained using a UV-vis spectrophotometer (Make – PerkinElmer Lambda 25 UV/Vis spectrometer in the wavelength range of 1100–190 nm with a 10 mm quartz cuvette at room temperature). All samples were diluted with hexane to obtain the absorbance in the quantifiable range of the spectrophotometer. Hexane, in the quantity of 9.9 ml, was mixed with 0.1 ml of the sample to prepare the final sample. The NMR spectra of all the samples were obtained using $CDCl_3$ as a solvent. Moreover, 0.1 ml of each sample was dissolved in 1 ml of the solvent.

2.1 Experimental procedure

The test was performed using a single cylinder four-stroke CRDI diesel engine. The fuel was directly injected into the combustion chamber of the diesel engine. The performance and emission results were obtained using six different rpm at a full load (30 N m). Cooling was achieved by a water system (a water-cooled engine). The fuel was maintained at a high pressure (300 bar) in the common rail from where it was forced into the injector nozzles of each cylinder. The fuel injection parameters could be varied using an electronic control unit (ECU). The file image of the CRDI engine is depicted in Fig. 1. A water-cooled eddy current dynamometer was used to achieve variation in the engine loading conditions. A strain gauge-type load cell was used for sensing the load (torque). The detail engine specification is shown in Table 1. The physiochemical characteristics of SME and its blends are provided in Table 2.

3. Result and discussion

3.1 FTIR spectroscopy

The FTIR spectra of MO-100, S80-M20, S70-M30, S50-M50, S-100 and diesel are presented in Fig. 2. The FTIR C=O signal area (1690–1800 cm^{-1}) was used for the determination of methyl in the biodiesel-diesel blends. The peaks in the spectral region from 1800 to 1700 cm^{-1} are due to the stretching of C=O, typical of esters, and present in FAME, S-100 and all blends; the spectral signals at 1460–1300 cm^{-1} correspond to the asymmetric $-CH_3$ stretching and bending;[5] the peaks of alcohol in the range from 3050 to 3600 cm^{-1} are absent in S70-M30; this indicates the absence of residual alcohol.[23] The peak between 3300 and 3600 was attributed to the axial –O–H and present in the cases of MO-100, S80-M20, S50-M50 and S-100; in the spectra of MO-100, S80-M20, and S50-M50, the peak around 2927 was attributed to $-C-H_2$. The peak at 1750 cm^{-1} was attributed to C=O, and the peak at 1747 cm^{-1} was attributed to the strong ester carbonyl bond stretching, indicating the presence of FAME; the spectra of all samples showed triglyceride ester linkages at 1745 cm^{-1}; the peak at 1746 cm^{-1} was changed, and the C=O stretching band shifted to a lower wavenumber (1743.65); this indicated an increase in the degradation of the biodiesel blends with MO. The peaks in the range from 725 cm^{-1} to 1161 cm^{-1} correspond to aromatic hydrocarbons, whereas those in the range from 1160 cm^{-1} to 1234 cm^{-1} correspond to C–O bond absorption;[24]

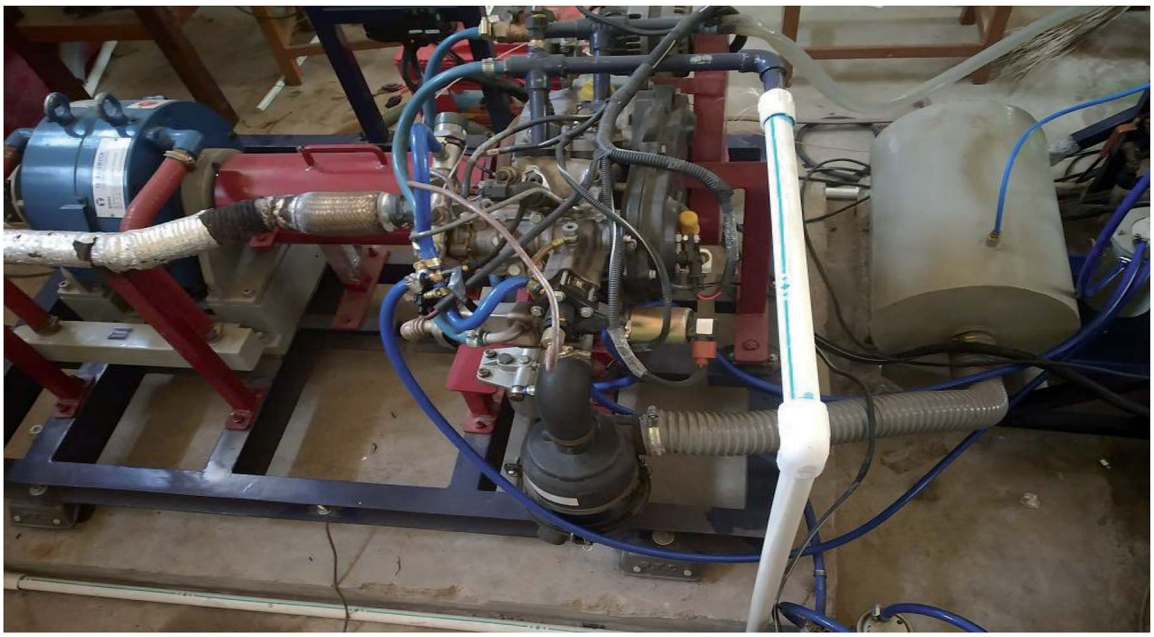

Fig. 1 CRDI engine setup.

Table 1 Specifications of the engine

Sl no.	Item	Specification
1	Manufacturer	Mahindra & Mahindra
2	Engine capacity (cm^3)	625
3	Cylinder (S)	1
4	Stroke (S)	4
5	Compression ratio (cr)	18 : 1
6	Bore (mm)	93.0–93.018
7	Stroke (mm)	92
8	Ignition	Compression
9	Max. power @ rpm	6.7 kW @ 3000 rpm
10	Max. torque @ rpm	30 N m @ 1800 rpm
11	Cooling system	Water cooled
12	No. of valves/cylinder	2

the absorption peak at 1373 cm^{-1} corresponds to the CH group, and the peak at 1458 cm^{-1} corresponds to the bending absorption of CH_2. The spectrum of each sample has peaks in the range from 2800 to 3000 cm^{-1}, corresponding to C–H; in the spectra of MO-100, the peak at 1194 cm^{-1} represents the stretching of O–CH_3, which is characteristic of FAME. The spectra of MO-100 and S50-M50 have a peak of –$COOCH_3$ at 1460 cm^{-1}. The IR spectra of S-100 and MO-100 show a strong peak of the ester at 1234 cm^{-1} (C–O vibrations). Moreover, the peak ranging from 1195 to 1246 cm^{-1} is attributed to –C–O–C– present in MO-100.[25] No interruptions were observed in the 1750 cm^{-1} region; however, the signals from diesel interfered with those in the 1170–1200 cm^{-1} region. All peaks of diesel were present in MO-100; the peaks observed at 2669 cm^{-1} in the spectra of diesel, S100, S70-M30 and S50-M50, 2727 cm^{-1} in the spectra of diesel and 3100–2700 cm^{-1} in the spectra of all the samples were attributed to the absorption of C–H bonds.[26]

3.2 UV spectroscopy

In the current study, UV-vis spectroscopy was conducted to investigate the diesel, S-100, MO-100, S80-M20, S70-M30 and

Table 2 Physiochemical properties of fuels

Properties	Test method	S-100	S80-M20	S70-M30	S50-M50	MO-100	Diesel
Density (kg m^{-3})	ASTM D1298	875.12	871.50	855.20	840.00	859.02	810.00
Viscosity (mm^2 s^{-1})	ASTM D445	4.78	4.64	4.63	4.56	4.34	3.18
Lower calorific value (MJ kg^{-1})	ASTM D240	34.69	34.79	34.92	35.25	37.05	42.50
Pour point (°C)	ASTM D97	−4	−6	−6	−9	−13	−20
Cloud point (°C)	ASTM D2500	12	11	10	4	6	−5
Flash point (°C)	ASTM D93	98	109	112	118	154	51
Fire point (°C)	ASTM D93	103	112	116	120	161	56
Initial boiling point (°C)		280	295	300	310	340	180
Carbon (%)	—	76.14	76.21	76.27	76.34	77.32	86.23
Hydrogen (%)	—	11.75	11.61	11.66	11.61	11.38	13.14
Oxygen (%)	—	12.11	12.18	12.07	12.05	11.30	—

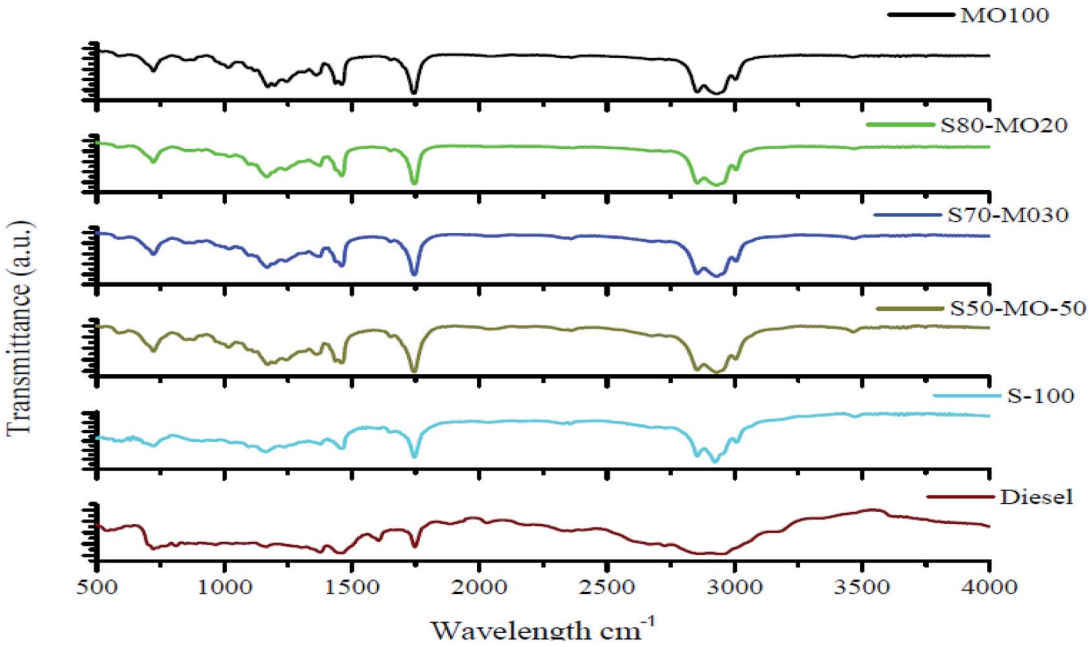

Fig. 2 FTIR spectra for diesel, S-100, MO-100, S80-M20, S70-M30 and S50-M50.

S50-M50 samples, indicating the presence of conjugated dienes in the oxidized biodiesel sample. The absorbance of biodiesel at each wavelength decreased due to dilution with an aliphatic compound such as MO (Fig. 3). The biodiesel blends during degradation and the double bonds in unsaturated FAME isomerized to form C=C–C=C or C=C–C=O.[27] The oxidation products with a conjugated double bond also absorbed energy in the ultraviolet and visible regions. S-100 and S70-M30 have low absorption coefficients in the region 245–275 nm but exhibit an abrupt increase in the absorption possibly due to the formation of α,β-unsaturated aldehydes or ketones with a conjugated double bond in the molecule.[28] Fang and McCormick have pointed that due to aldol-condensation reactions at the later stage of oxidation, oligomers of different types are produced.[29]

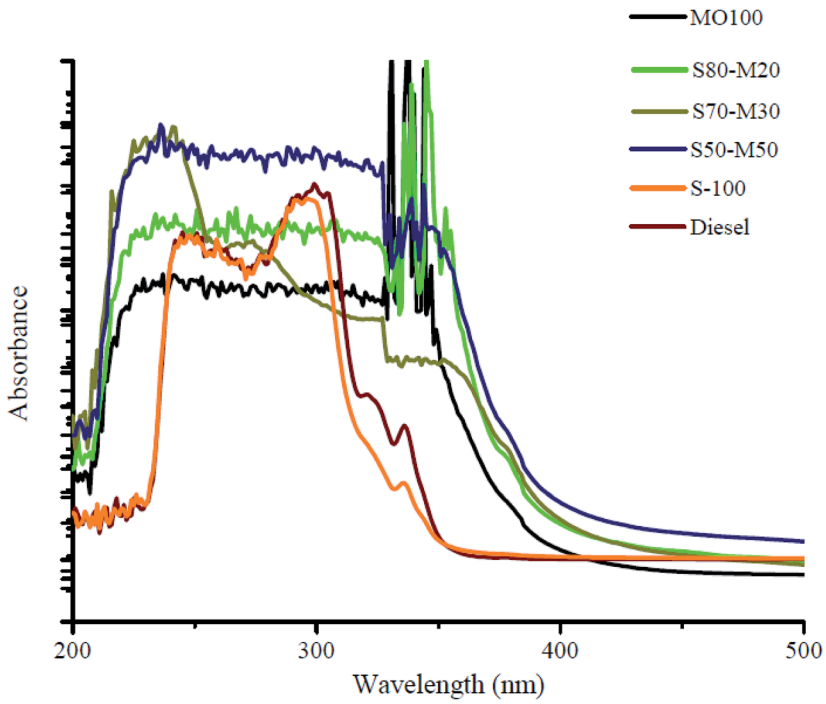

Fig. 3 UV-vis spectra of diesel, S-100, MO-100, S80-M20, S70-M30 and S50-M50.

In the presence of both linoleic acid and methyl ester, the fully saturated and monounsaturated FAAE in the UV region are not absorbed strongly, whereas polyunsaturated samples are absorbed strongly and have characteristic spectra.[30] S-100 absorbed least and MO-100 samples showed highest absorbance.

The linearity of absorbance decreased with an increase in blending; this was due to a decrease in the concentration of aliphatic compounds (Fig. 4). The linear line fitted for absorbance *versus* percentage of biodiesel at 320 nm shows a high coefficient of determination ($R^2 = 0.9454$).

3.3 NMR spectrum characterization

The samples S70-M30, MO-100, S50-M50 and S80-M20 showed a characteristic singlet peak at 3.6 ppm mainly due to the methyl ester moiety. The presence of peaks at 3.62 ppm in the spectrum of MO-100, 3.60 ppm in the spectrum of S80-M20, 3.64 ppm in the spectrum of S70-M30 and 3.59 ppm in the spectrum of S50-M50 makes them distinguishable from diesel (Fig. 5A–E); the triplet at around 0.8 ppm is due to methyl hydrogen, whereas the peak at 4.0–4.5 is due to glyceryl groups and present in MO-100, S80-M20, S70-M30 and S50-M50. The spectra of S-100 exhibited peak at 1.2 ppm and 1.59 (Fig. 5E) and 1.59 ppm due to the methylene group of the carbon chain and beta-carbonyl methylene, respectively; the signals of –OC=O–CH_2 (triplet of CH_2 by the carbonyl group of the ester moiety) are present in the spectra of all S and MO mixtures at around 2.28 ppm.[9] In the spectra of S-100, the peaks located at 2.0, 2.77 and 5.32 ppm are attributed to allylic, bis-allylic and olefinic hydrogen, respectively (Fig. 5E).

The NMR spectrum (Fig. 5F) of diesel showed a group of peaks at 0.8–2.8 ppm, which originated from aliphatic hydrogens, and quite a few peaks in the 6.79–7.25 ppm range, which originated from aromatic hydrogens. Table 3 presents the functional groups and their respective peaks in ppm in the spectra of the samples.[9]

3.4 Brake power (BP)

The variation of BP with respect to engine speed at full load is illustrated in Fig. 6. When the load was kept constant at a full load and the engine speed was varied from 1500 to 3000 rpm (Max. speed), BP was found to increase with an increase in the engine speed for pure diesel, SME and MO biodiesel-blended fuels. An increase in the engine speed leads to an increase in the flow rate of the aspirated air; thus, the BP tends to increase. Moreover, at lower speeds, more heat loss occurred through the combustion chamber, whereas at higher speeds, lesser heat transfer occurred, which led to high BP. The average BP values were found to be 2.4% (MO-100), 13% (S-100), 10.5% (S80-M20), 8.79% (S70-M30) and 4.9% (S50-M50) lower than that of the diesel fuel. The BP for pure diesel was highest among all other fuels at all engine speeds. The decrease in the BP of biodiesels was due to their lower calorific value. Moreover, the higher viscosities of the biodiesels lead to poor combustion. There were no significant changes in the BP at a particular speed for biodiesels and its blends.

3.5 Brake thermal efficiency (BTE)

The variation of the BTE with engine speed at full load is illustrated in Fig. 7. The BTE of pure diesel has been found to be highest among all the fuels at all speeds. However, the BTE for pure diesel has been found to significantly increase till 2400 rpm, after which it starts to decrease. This is due to the lack of mixing at higher speeds.[31] MO-100 also shows a similar trend as pure diesel. Since the BSFC of the biodiesels was decreased by enriching them with MO, the BTE of the biodiesel blends had improved. At full load, the average BTE values were found to be 6.8% (MO), 18.4% (S-100), 17.2% (S80-M20), 12.7% (S70-M30) and 9.8% (S50-M50) lower

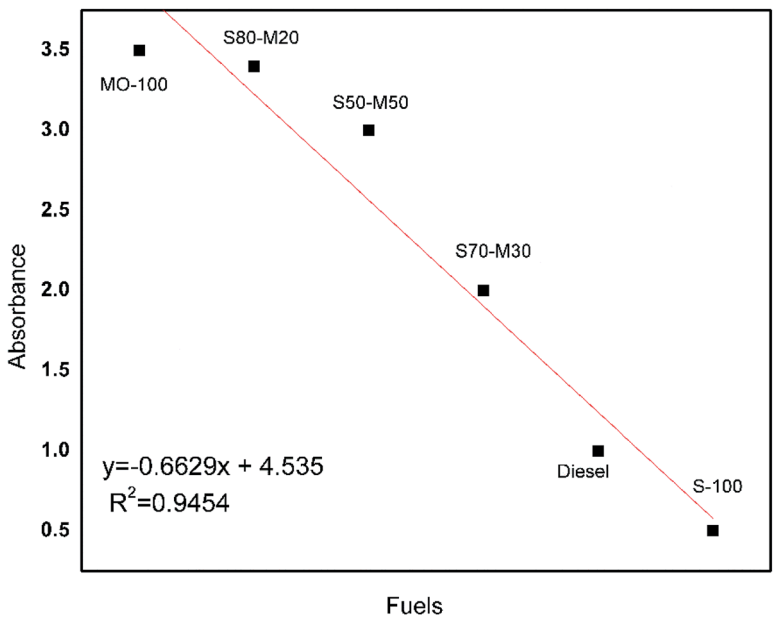

Fig. 4 Absorbance of diesel and blended biodiesel with MO.

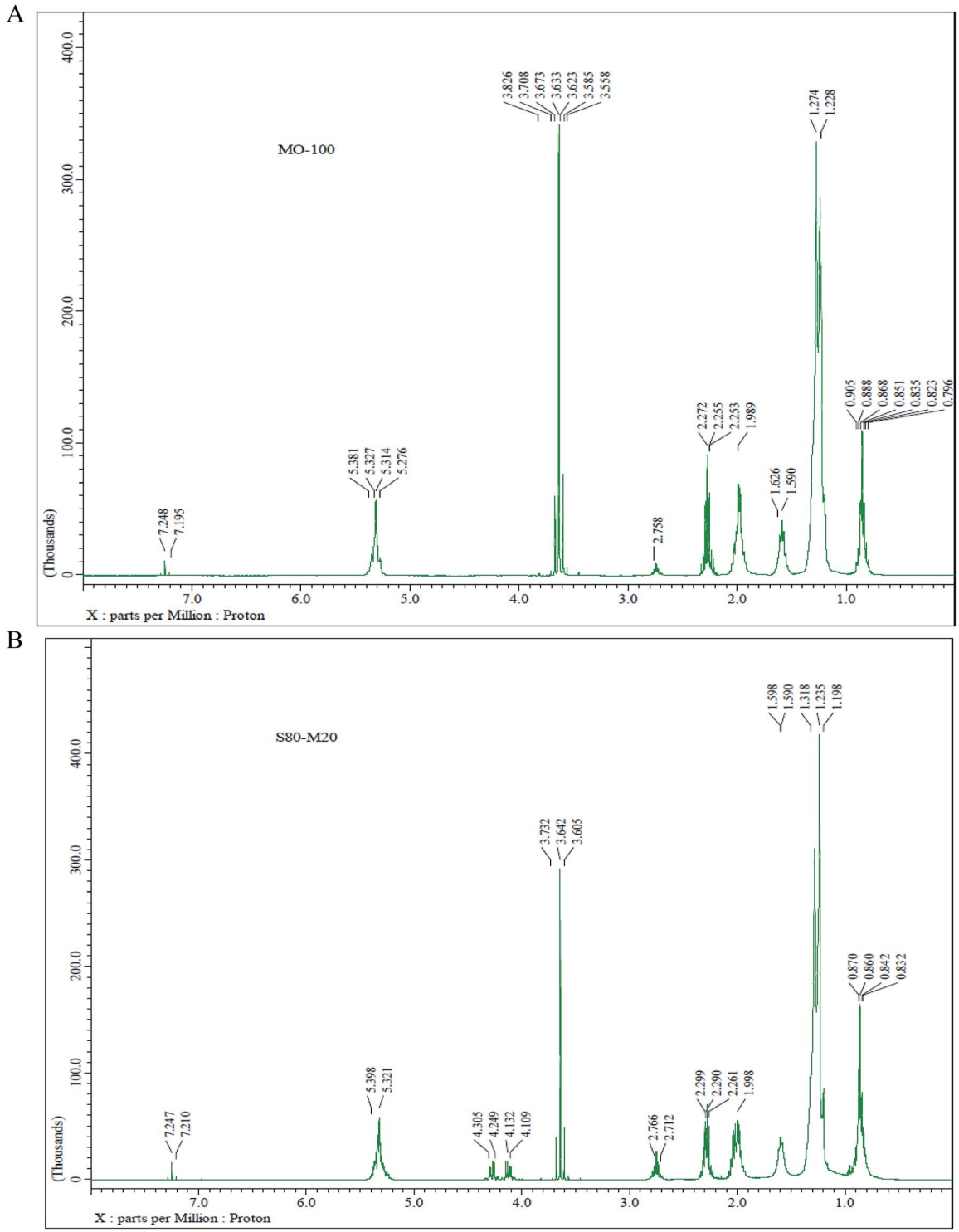

Fig. 5 (*contd.*)

than that of the diesel fuel. The BTE for S-100 is lesser than that of diesel at all engine speeds. This is due to low CV of soybean. For the same reason, the BTE of the enriched biodiesel is lower than that of the pure diesel. Moreover, there is an increase in the BTE for enriched biodiesels as compared to the case of S-100 because of the reduced kinematic viscosity, which leads to better atomization and vaporization.

3.6 Brake specific fuel consumption (BSFC)

The variation of BSFC with the engine speed at full load is depicted in Fig. 8. The BSFC first decreases and then slightly increases with an increase in the engine speed after 2400 rpm for diesel oil. At full load, the average BSFC values were found to be 7.9% (MO-100), 30.1% (S-100), 26.5% (S80-M20) 17.6%

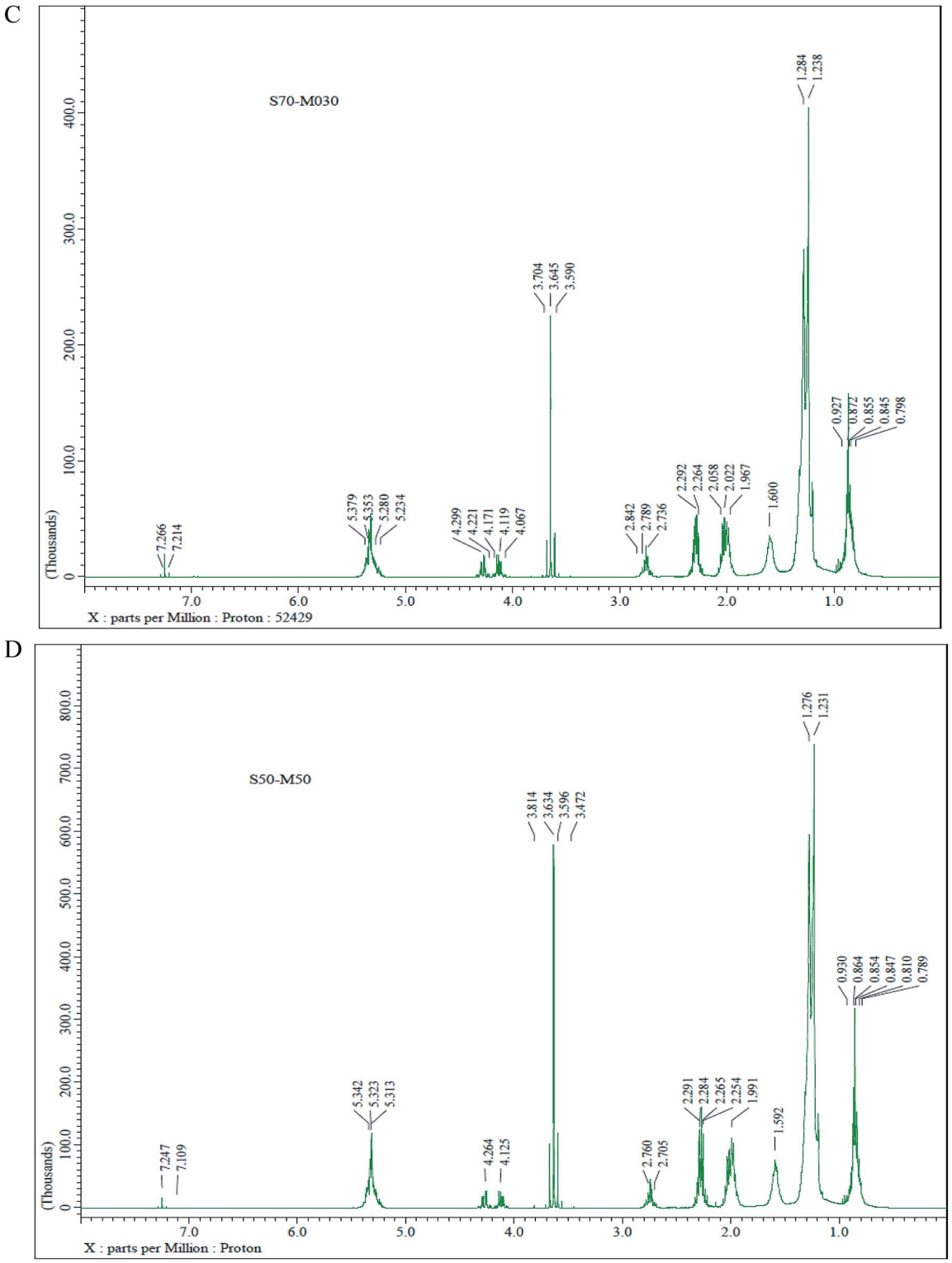

Fig. 5 (*contd*.)

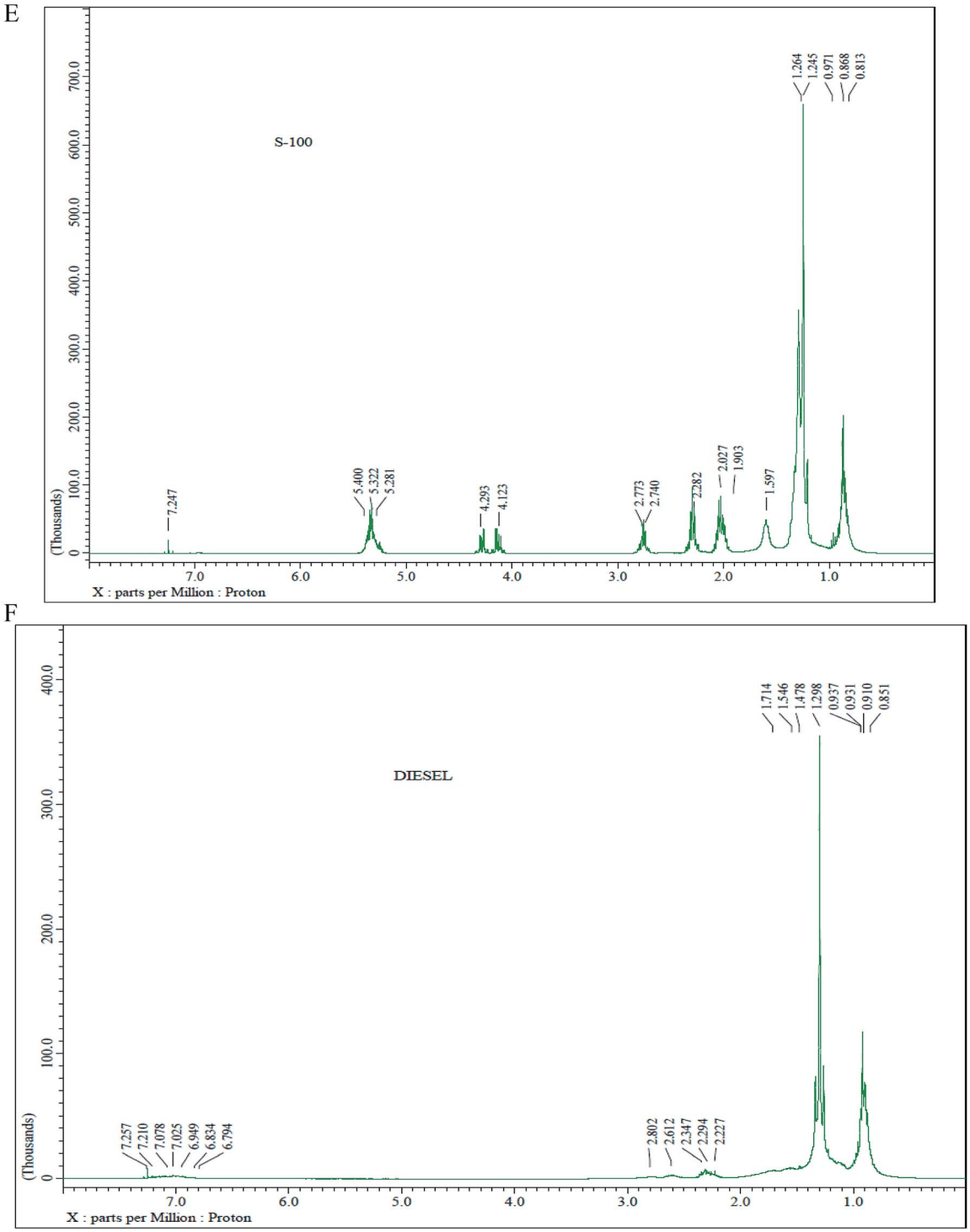

Fig. 5 (A) ^{1}H NMR spectrum of MO-100; (B) ^{1}H NMR spectrum of S80-M20; (C) ^{1}H NMR spectrum of S70-M30; (D) ^{1}H NMR spectrum of S50-M50; (E) ^{1}H NMR spectrum of S-100; (F) ^{1}H NMR spectrum of diesel.

(S70-M30) and 15% (S50-M50) higher than that of the diesel fuel. The BSFC of neat MO was found to be higher than that of diesel at all speeds, and the BSFC of S-100 was highest. This was due to lower energy densities of the biodiesels, which caused the combustion of more quantity of fuel for the same power output. For the same reason, the S-100 and MO-enriched samples also yielded higher BSFC than the pure diesel at all engine speeds. The BSFC for S-100 tended to decrease with an increase in the engine speed; this was due to its high oxygen content. Among the enriched biodiesels, BSFC was found to improve with an increase in the blend quantity of MO in S-100 at all engine speeds.

Table 3 Functional groups and their respective peaks in ppm in the spectra of samples

Sample's where peaks are present	Functional group	ppm
MO-100, S80-M20, S70-M30, S50-M50, S-100, diesel	$-CH_2-CH_3$	0.84–0.90
MO-100, S80-M20, S70-M30, S50-M50, S-100, diesel	$-CH_2-CH_3$	0.93–1.29
MO-100, S80-M20, S70-M30, S50-M50, S-100	$-OCO-CH_2-CH_2$	1.54–1.71
MO-100, S80-M20, S70-M30, S50-M50, S-100, diesel	$-CH_2-C=C-$	1.96–2.15
MO-100, S80-MO20, S70-MO30, S50-M50, S-100	$-OC=O-CH_2$	2.28
MO-100, S80-M20, S70-M30, S50-M50, S-100, diesel	$C=C-CH_2-C=C$	2.75–2.83
MO-100, S80-M20, S70-M30, S50-M50	$-COOCH_3$	3.64–3.68
S80-MO20, S70-MO30, S50-M50, S-100	$-CH_2OCOR$	4.0–4.5
MO-100, S80-M20, S70-M30, S50-M50, S-100	$-CH=CH-$	5.24–5.42

3.7 NO_x emission

The variation in the concentration of NO_x with engine speed for different fuels is illustrated in Fig. 9. The concentration of NO_x decreased with an increase in the engine speed due to lesser available time for the formation of NO_x as the flow velocity of the fresh air–fuel mixture and the volumetric efficiency increased.[35] The enriched biodiesels yielded more NO_x emission as compared to diesel at all engine speeds. This was because the higher oxygen content of the enriched biodiesels caused complete oxidation, resulting in high in-cylinder temperature and NO_x emission. At full load, the average NO_x values were found to be 8.3% (S-100), 13.8% (S80-M20), 14.6% (S70-M30), 15.8% (S50-M50) and 18.8% (MO-100) higher than that of the diesel fuel. For the tested fuels, the NO_x level increased with an increase in the blend concentration of MO because of an increase in the degree of unsaturation.[32,33] For the same reason, NO_x emission was found to be highest for MO-100 at all engine speeds. Low degree of unsaturation causes shorter ID, which leads to lesser combustion in the pre-mixed phase, and thus, lower combustion rates and low NO_x are observed.[34]

3.8 CO_2 emission

The variation in the concentration of CO_2 with the engine speed for different fuels is illustrated in Fig. 10. The concentration of CO_2 was found to decrease with an increase in the engine speed for all tested fuels. Moreover, the CO_2 level was lowest for diesel. At full load, the average CO_2 values were found to be 7.7% (MO-100), 27.5% (S-100), 21.7% (S80-M20), 16.6% (S70-M30) and 13.1% (S50-M50) higher than that of the diesel fuel. At all engine speeds, the concentration of CO_2 for enriched biodiesels was higher than that for the diesel because of the presence of higher oxygen content in them that accounted for the complete combustion of fuel. Moreover, the CO_2 level was found to be highest for S-100 due to the highest content of oxygen in it.

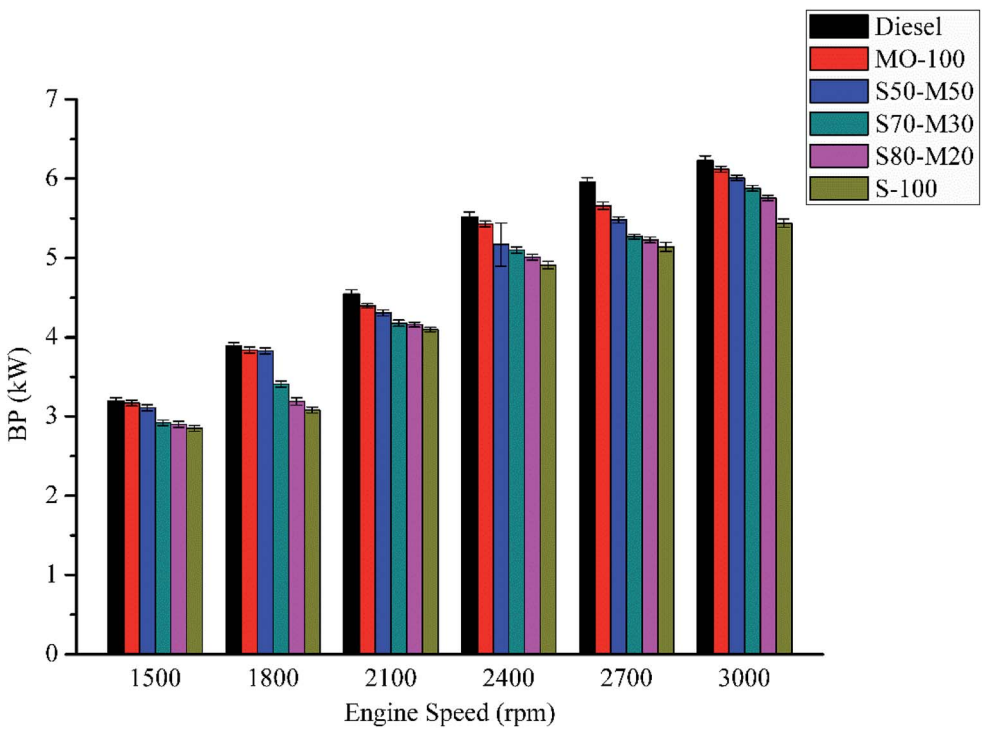

Fig. 6 Variation of BP with engine speed at full load.

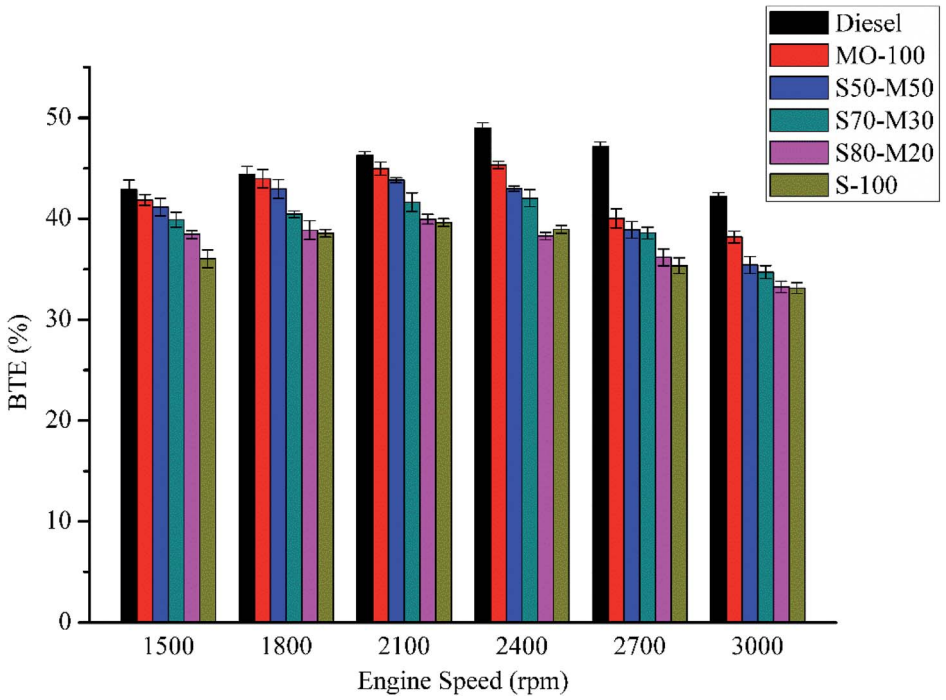

Fig. 7 Variation of the BTE with engine speed at full load.

3.9 CO emission

The variation in the concentration of CO with the engine speed for different fuels is illustrated in Fig. 11. The concentration of CO depends on the speed of the engine, the quality of the fuel used and the A/F. The concentration of CO was found to decrease from 1500 rpm to 2100 rpm and then increase from 2400 rpm to 3000 rpm. The decrease in the CO level with an increase in the engine speed was due to the complete combustion of fuel attributed by the better intermixing of air and fuel at higher speeds.[35] On the contrary, the increase in the concentration of CO from 2400 rpm onwards was due to an increase in the combustion rate, which demanded a richer mixture. At full load, average reduction in the CO value was found to be 67% (S-100), 52.4% (S80-M20), 48% (S70-M30), 44.3% (S50-M50) and 33% (MO-100)

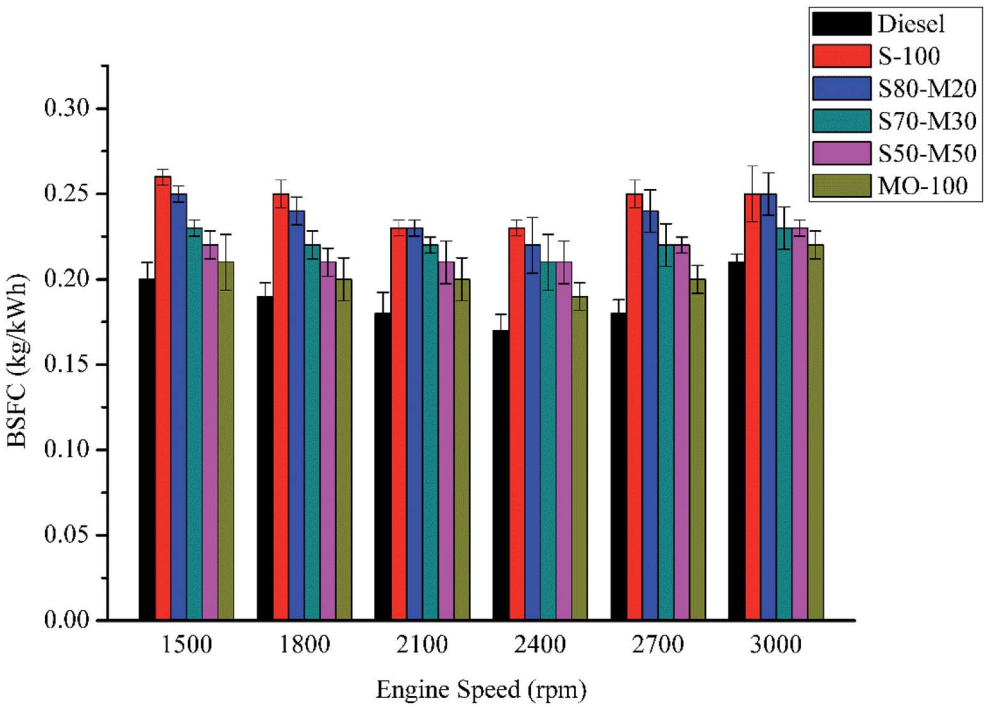

Fig. 8 Variation of the BSFC with engine speed at full load.

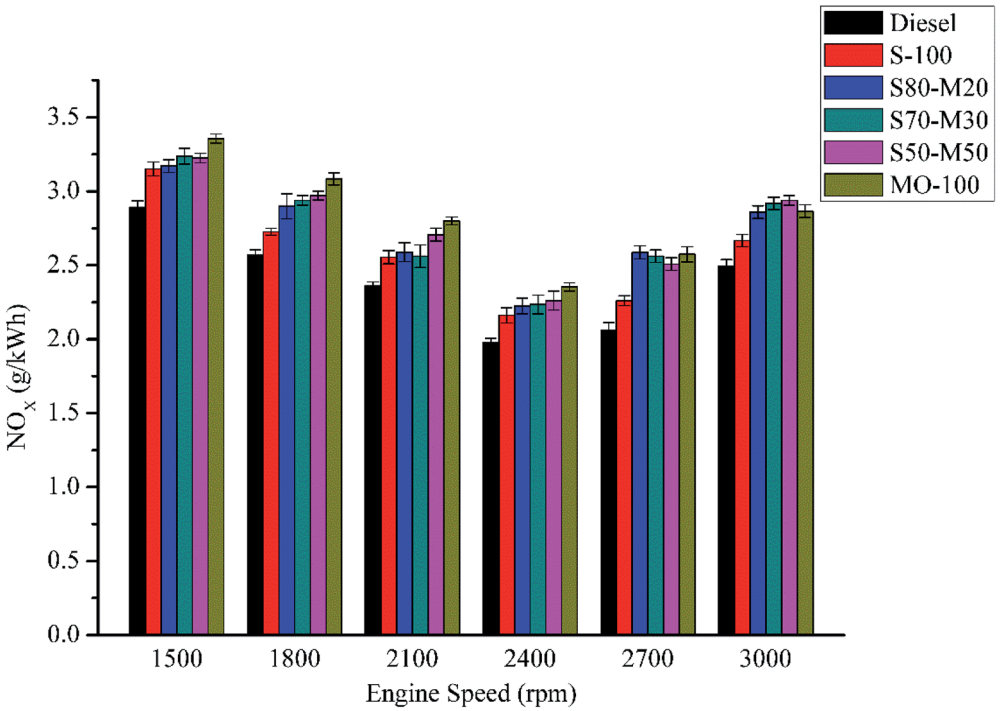

Fig. 9 Variation in the NO_x concentration with engine speed at full load.

lower than that for the diesel fuel. The CO level of diesel was highest at all engine speeds because the rest of the fuels had more oxygen content than diesel and thus underwent complete combustion. In general, at any particular speed, the CO emission of the biodiesel blends was found to increase with an increase in the concentration of MO. However, a slight exception was observed at 2100 rpm and 3000 rpm. The CO emissions of the tested blends were higher than that of S-100 because the blends had lower oxygen content than SME, which triggered incomplete combustion.

3.10 Unburnt hydrocarbon (UHC)

The variation in the concentration of UHC with the engine speed for different fuels is illustrated in Fig. 12. The UHC

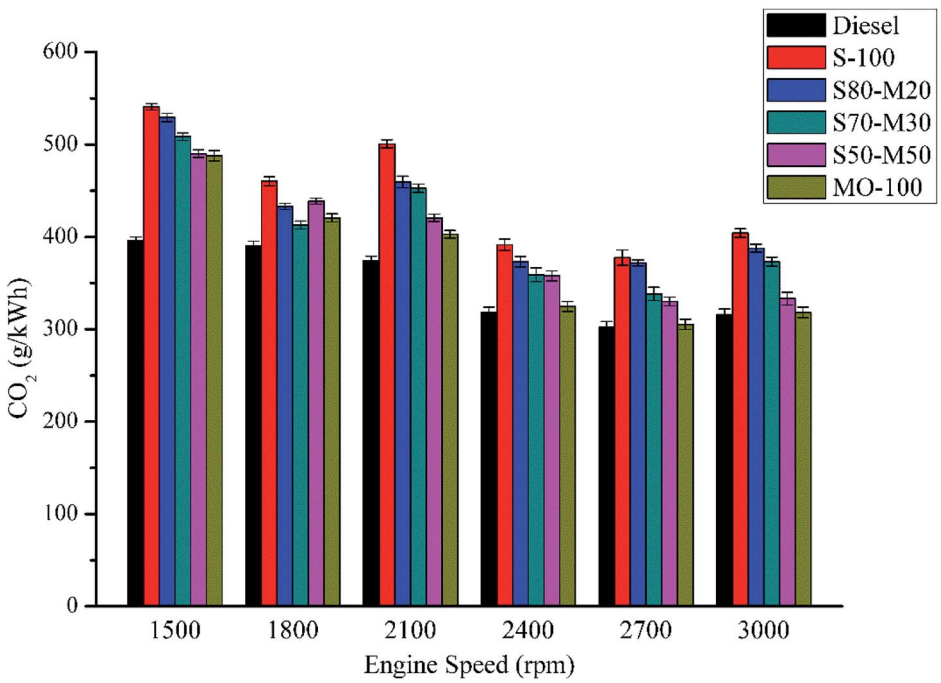

Fig. 10 Variation in the concentration of CO_2 with engine speed at full load.

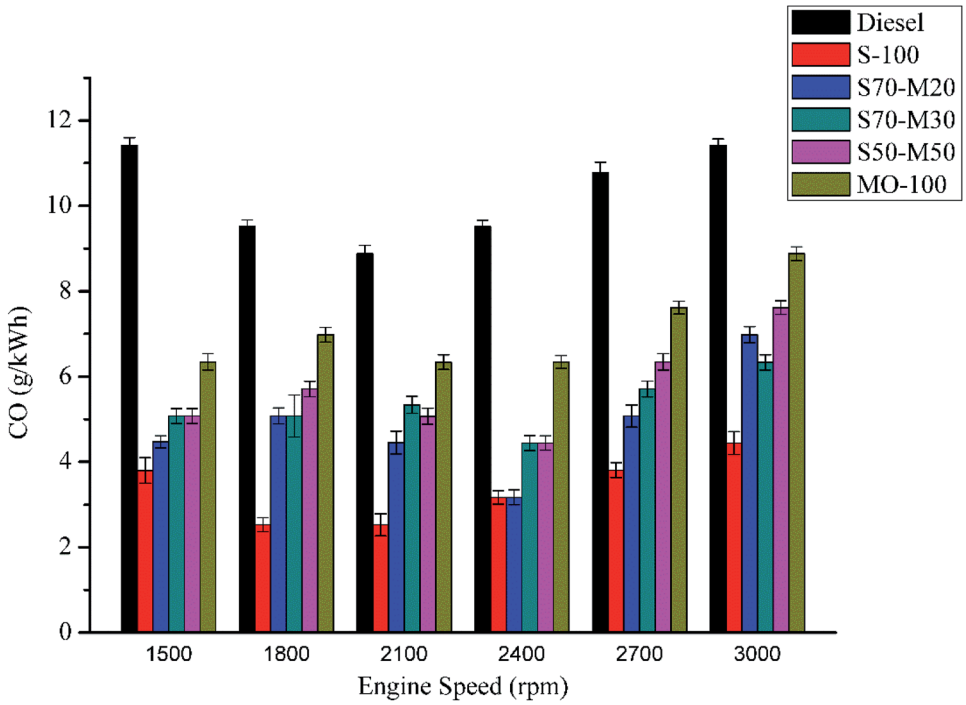

Fig. 11 Variation in the CO concentration with engine speed at full load.

emission level was found to decrease with an increase in the engine speed from 2400 to 3000 rpm for all tested fuels due to improved intermixing at higher speeds. The enriched biodiesels showed lower UHC emission than the pure diesel at all engine speeds due to their higher oxygen contents, which caused complete combustion of the fuel. S-100 showed least UHC emission as it had highest oxygen content. At full load, the average reduction in the UHC value was found to be 52.8% (S-100), 49.7% (S80-M20), 42.6% (S70-M30), 37.7% (S50-M50) and 36.1% (MO-100) lower than the diesel fuel. Moreover, among the tested blends, the concentration of UHC increased with an increase in the concentration of MO due to the corresponding reduction in the cetane number and oxygen content by mass fraction.[36,37]

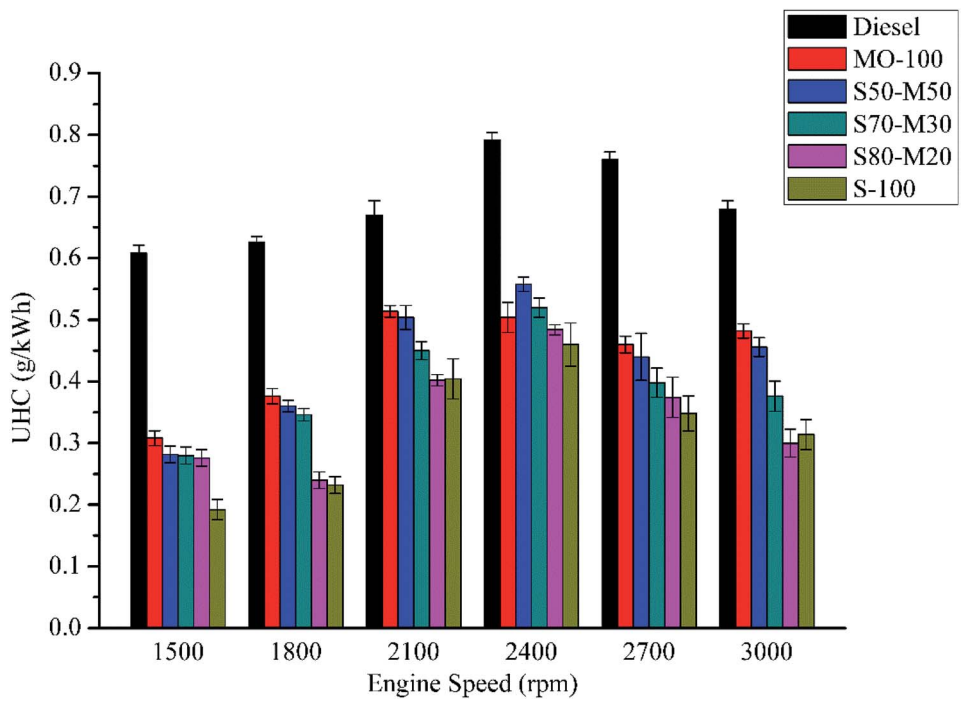

Fig. 12 Variation of the concentration of UHC with engine speed at full load.

4. Conclusion

The performance and emission tests of an SME blended with MO indicated that this blend was an enriched biodiesel. The results indicated a reduction in the BSFC and an increase in BTE for the blended biodiesel (S80-M20, S70-M30, and S50-M50) with respect to the case of SME. MO blending resulted in oxidative stability, better ignition quality, and low-temperature flow properties. There were also a remarkable balance between oxidative stability and low flow properties. An increase in the concentration of MO in SME led to a decrease in the CO_2 emissions by facilitating incomplete combustion. UHC also increased upon enriching SME with MO as the oxygen content decreased, leading to more incomplete combustion. The NO_x emission increased with an increase in the ratio of MO in SME because of the presence of unsaturated fatty acids in MO. Thus, S70-M30 and S80-M20 may be considered as optimal fuels for use as blended fuels in engine. The FTIR spectra indicated the presence of a triglyceride ester linkage at 1745 cm^{-1}; the peaks in the spectral region from 1800 to 1700 cm^{-1} originated from the esters and were present in the spectra of FAME, S-100 and all blends. The UV-vis absorption of the biodiesel was in the range from 240 to 340 nm, and the linearity showed a high coefficient of determination (R^2 = 0.9454); the NMR spectra showed a signal at 3.6 ppm due to the methyl ester moiety, a triplet at around 0.8 ppm due to methyl hydrogen, and a triplet at around 2.28 ppm due to carbonyl methylene. The characterization techniques displayed the quantification of different blends of biodiesel. In the future, the oxidative stability and molecular interactions of the blended biodiesel will be analyzed using the NMR technique.

Conflicts of interest

The authors have no conflict of interests. The funders had no role in the design of the study, in the collection, analyses, or interpretation of data, in the writing of the manuscript, or in the decision to publish the results.

Acknowledgements

This study was supported by the Department of Mechanical Engineering and Central Instrumentation Facility, Birla Institute of Technology, Mesra, Ranchi, Jharkhand, India.

References

1 S. S. Pantoja, L. R. V. da Conceição, C. E. da Costa, J. R. Zamian and G. N. da Rocha Filho, *Energy Convers. Manage.*, 2013, **74**, 293–298.
2 G. Karavalakis and S. Stournas, *Energy Fuels*, 2010, **24**(6), 3682–3686.
3 P. Bondioli, A. Gasparoli, L. Della Bella, S. Tagliabue and G. Toso, *Eur. J. Lipid Sci. Technol.*, 2003, **105**(12), 735–741.
4 K. Bacha, A. Ben-Amara, A. Vannier, M. Alves-Fortunato and M. Nardin, *Energy Fuels*, 2015, **29**(7), 4345–4355.
5 F. Faraguna, M. Racar and A. Jukić, *Renewable Energy*, 2019, **133**, 1231–1235.
6 G. G. Shimamoto, L. F. Bianchessi and M. Tubino, *Talanta*, 2017, **168**, 121–125.
7 G. F. Ghesti, J. L. de Macedo, I. S. Resck, J. A. Dias and S. C. Dias, *Energy Fuels*, 2007, **21**(5), 2475–2480.
8 G. Knothe, *J. Am. Oil Chem. Soc.*, 2001, **78**(10), 1025–1028.
9 M. R. Monteiro, A. R. P. Ambrozin, L. M. Liao and A. G. Ferreira, *Fuel*, 2009, **88**(4), 691–696.
10 L. A. Anderson and A. K. Franz, *Energy Fuels*, 2012, **26**(10), 6404–6410.
11 J. K. Satyarthi, D. Srinivas and P. Ratnasamy, *Energy Fuels*, 2009, **23**(4), 2273–2277.
12 A. Monyem and J. H. Van Gerpen, *Biomass Bioenergy*, 2001, **20**(4), 317–325.
13 R. M. Joshi and M. Pegg, *J. Fuels*, 2007, **86**(1–2), 143–151.
14 G. R. Kannan, R. Karvembu and R. Anand, *Appl. Energy*, 2011, **88**(11), 3694–3703.
15 K. Gopal Radhakrishnan, *Environ. Eng. Sci.*, 2019, **36**(5), 589–603.
16 S. Ganesan, S. Mahalingam, R. A. Shyam Daniel Raj and S. Rajesh, *Int. J. Ambient Energy*, 2018, 1–4.
17 M. A. H. Altaie, *Biofuels*, 2017, 1–10.
18 A. Cardoso, S. Neves and M. Da Silva, *Energies*, 2008, **1**(2), 79–92.
19 K. A. Burdett, L. D. Harris, P. Margl, B. R. Maughon, T. Mokhtar-Zadeh, P. C. Saucier and E. P. Wasserman, *Organometallics*, 2004, **23**(9), 2027–2047.
20 P. S. Wang, J. Thompson, T. E. Clemente and J. H. T. Van Gerpen, *Trans. ASABE*, 2010, **53**(6), 1853–1858.
21 G. Knothe, *Fuel*, 2014, **119**, 6–13.
22 Y. B. Lai, Y. N. Yuan and X. Chen, *Adv. Mater. Res.*, 2012, **347**, 2651–2655.
23 S. N. Shah, A. Joshi, A. Patel and V. P. &Brahmkhatri, *Energy Power*, 2013, **3**(1), 7–11.
24 R. Chatterjee and S. K. Mukherjee, *Waste Biomass Valorization*, 2018, **9**(9), 1579–1585.
25 O. Berdeaux, S. Fontagné, E. Sémon, J. Velasco, J. L. Sébédio and C. Dobarganes, *Chem. Phys. Lipids*, 2012, **165**(3), 338–347.
26 M. Bradley, *Bio-diesel (FAME) Analysis by FT-IR*, 2007, available: http://www.thermo.com/eThermo/CMA/PDFs/Articles/articlesFile_2448.pdf.
27 T. Vega-Lizama, L. Díaz-Ballote, E. Hernández-Mézquita, F. May-Crespo, P. Castro-Borges, A. Castillo-Atoche and L. Maldonado, *Fuel*, 2015, **156**, 158–162.
28 G. G. Pereira, R. M. Alberici, G. D. Fernandes, I. B. Cunha, M. N. Eberlin, M. C. Dobarganes and D. Barrera-Arellano, *Eur. J. Lipid Sci. Technol.*, 2014, **116**(8), 952–960.
29 H. L. Fang and R. L. McCormick, *SAE Technical Paper*, 2006.
30 A. Zawadzki, D. S. Shrestha and B. He, *Trans. ASABE*, 2007, **50**(4), 1349–1353.
31 A. Datta and B. K. Mandal, *Clean Technol. Environ.*, 2018, **20**(8), 1773–1790.
32 C. S. Cheung, L. Zhu and Z. Huang, *Atmos. Environ.*, 2009, **43**(32), 4865–4872.

33 P. K. Devan and N. V. Mahalakshmi, *Appl. Energy*, 2009, **86**(5), 675–680.
34 P. Benjumea, J. R. Agudelo and A. F. Agudelo, *Energy Fuels*, 2010, **25**(1), 77–85.
35 C. Y. Lin and R. J. Li, *Fuel Process. Technol.*, 2009, **90**(7–8), 883–888.
36 M. A. H. Altaie, R. B. Janius, U. Rashid, Y. H. Taufiq-Yap, R. Yunus, R. Zakaria and N. M. Adam, *Energy Convers. Manage.*, 2015, **106**, 365–372.
37 F. Wu, J. Wang, W. Chen and S. Shuai, *Atmos. Environ.*, 2009, **43**(7), 1481–1485.